Cancer Science

WILEY

Cancer Science

ORIGINAL ARTICLE OPEN ACCESS

VRK1 Is a Novel Therapeutic Target for Small Cell Neuroendocrine Carcinoma of the Cervix

Mariya Kobayashi[1] | Satoshi Nakagawa[1] | Yusuke Ishii[1] | Yuji Kamei[1,2] | Mizuki Kanda[1,3] | Tatsuo Masuda[1] | Mamoru Kakuda[1] | Kosuke Hiramatsu[1] | Tadashi Iwamiya[1] | Tomomi Egawa-Takata[4] | Shinya Matsuzaki[1] | Hiroyuki Uematsu[3] | Kunishige Onuma[3] | Masahiro Inoue[3] | Yutaka Ueda[1] | Tadashi Kimura[1,5] | Michiko Kodama[1]

[1]Department of Obstetrics and Gynecology, Graduate School of Medicine, The University of Osaka, Osaka, Japan | [2]Department of Obstetrics and Gynecology, Higashiosaka City Medical Center, Osaka, Japan | [3]Department of Clinical Bio-Resource Research and Development, Graduate School of Medicine, Kyoto University, Kyoto, Japan | [4]Department of Obstetrics and Gynecology, Kansai Rosai Hospital, Amagasaki, Hyogo, Japan | [5]Sakai City Hospital Organization, Osaka, Japan

Correspondence: Satoshi Nakagawa (s.nakagawa@gyne.med.osaka-u.ac.jp)

Received: 23 March 2025 | **Revised:** 15 September 2025 | **Accepted:** 18 September 2025

Funding: This work was supported in part by Osaka Prefecture Subsidy for the Promotion of the Medical Career Development Support Program for 2022, 2023, and 2024.

Keywords: cervical cancer | in vivo | mitochondria | small cell neuroendocrine carcinoma | VRK1

ABSTRACT

Small cell neuroendocrine carcinoma of the cervix (SCNEC) is classified as a high-grade neuroendocrine carcinoma with a worse prognosis than other major histological types of cervical cancer. Identifying novel therapeutic targets based on its molecular characteristics is highly desirable but challenging due to the rarity of SCNEC and the resulting lack of research resources. In this study, we identified vaccinia-related kinase 1 (VRK1) as a potential therapeutic target for SCNEC. VRK1 was prioritized based on our previously reported proteomic analysis of patient-derived organoids. Immunohistochemistry of patient samples consistently revealed high VRK1 expression in SCNEC, as opposed to its variable expression in other cervical carcinomas. Although VRK1 knockdown in SCNEC had only a limited effect on cell proliferation in two-dimensional cultures, it significantly suppressed cell proliferation in three-dimensional cultures and inhibited xenograft tumor growth in vivo. Gene set enrichment analysis of RNA-sequencing data from mouse xenograft models demonstrated that VRK1 is associated with mitochondrial-related pathways. Furthermore, under oxidative stress conditions, VRK1 knockdown resulted in a reduction of mitochondrial membrane potential, an indicator of mitochondrial integrity, and decreased expression of cytochrome c oxidase subunit IV (COX IV), a nuclear-encoded subunit of cytochrome c oxidase, the terminal enzyme complex of the mitochondrial respiratory chain. These findings suggest that VRK1 knockdown indirectly impaired mitochondrial function. Collectively, these anti-tumor effects highlight VRK1 as a promising therapeutic target for SCNEC.

Abbreviations: 2D, two-dimensional; 3D, three-dimensional; AC, adenocarcinoma; COX, cytochrome c oxidase; COX IV, cytochrome c oxidase subunit IV; DMEM, Dulbecco's Modified Eagle's medium; GEO, Gene Expression Omnibus; GO, Gene Ontology; GSEA, gene set enrichment analysis; H_2O_2, hydrogen peroxide; HPA, Human Protein Atlas; HPV, human papillomavirus; OS, overall survival; RNA-seq, RNA-sequencing; ROS, reactive oxygen species; SCC, squamous cell carcinoma; SCLC, small cell lung cancer; SCNEC, small cell neuroendocrine carcinoma of the cervix; shRNA, short hairpin RNA; VRK1, vaccinia-related kinase 1.

1 | Introduction

Cervical cancer is the fourth most common cancer in women, with 662,301 new cases (age-standardized rate: 14.1 per 100,000) and 348,874 deaths (age-standardized rate: 7.1 per 100,000) reported worldwide [1]. Small cell neuroendocrine carcinoma of the cervix (SCNEC) is classified as a high-grade neuroendocrine carcinoma and has a worse prognosis than other major histological types of cervical cancer, such as squamous cell carcinoma (SCC) and adenocarcinoma (AC). The overall 5-year survival (OS) rate for cervical cancer is approximately 70%, whereas the stage-specific 5-year OS rates for SCNEC are 56.7%, 41.0%, 27.6%, and 5.3% for stages I, II, III, and IV, respectively [2–7].

Regarding the treatment of SCNEC, chemotherapy plays a crucial role due to its aggressive nature, with a high proportion of patients presenting with metastatic disease [2, 5, 8–9]. However, SCNEC is rare, accounting for only approximately 1% of all cervical cancers, resulting in a lack of basic research and Level I evidence [4, 5, 7]. As a result, chemotherapy for SCNEC has traditionally been adapted from those used for small cell lung cancer (SCLC), the most common primary site of small cell neuroendocrine carcinoma [7, 10–11]. Nevertheless, there are notable distinctions between SCNEC and SCLC. These include differences in the mechanisms of p53 and RB1 inactivation (genetic mutations in SCLC vs. HPV-mediated inactivation in SCNEC), the spectrum and frequency of gene mutations, and tumor mutational burden values [12–16]. Therefore, SCLC-based management of SCNEC may be suboptimal for SCNEC, highlighting the need to identify therapeutic targets or biomarkers tailored to the unique molecular characteristics of SCNEC [7].

Multi-omics sequencing and immunohistochemistry revealed that the RNA expression profiles of SCNEC closely resemble those of other small cell neuroendocrine carcinomas, such as SCLC and small cell carcinoma of the bladder, rather than those of other common types of cervical cancers like SCC and AC [12]. Similar results were obtained in our previous proteomic analysis using isobaric tags for relative and absolute quantitation of patient-derived organoids, which compared protein expression across various histological types of lung and cervical cancers. In this analysis, we identified 16 proteins that were characteristically overexpressed in SCNEC compared to SCC and AC [11]. Among these, this study focused on vaccinia-related kinase 1 (VRK1), a protein reported as a therapeutic target in other cancers and with potential for drug development.

VRK1 is a member of the VRK family of serine/threonine kinases, and it is significantly upregulated in various human malignancies compared to normal tissues [17–19]. High VRK1 expression is associated with poor prognosis across multiple cancer types and has thus attracted attention as a promising therapeutic target, for which a novel and specific inhibitor has been recently developed [20–28]. Functionally, VRK1 plays a role in cell cycle progression and in the cellular responses to stress signals, including oxidative stress-induced DNA damage, by regulating chromatin remodeling and transcription factors such as p53, Sox2, ATF2, CREB, and c-JUN [20–27, 29–30]. VRK2, another member of the VRK family and a paralog of VRK1, has been reported as a biomarker for effective targeting of VRK1 [26, 27].

In this study, we identified SCNEC as a tumor type characterized by high VRK1 expression, in contrast to its variable expression in other common types of cervical cancers. VRK1 knockdown suppressed tumor growth in SCNEC both in three-dimensional (3D) culture conditions and in vivo. Mechanistically, this effect appears to be mediated by indirect mitochondrial dysfunction. These findings suggest that VRK1 could serve as a promising therapeutic target for SCNEC.

2 | Material and Methods

Detailed information can be found in Data S1.

2.1 | Patients and Clinical Samples

Tissue samples were obtained from patients with SCC and AC of the uterine cervix who underwent treatment in 2023, as well as from patients with SCNEC who underwent treatment between 2015 and 2024. Samples collected after chemotherapy or radiotherapy were excluded. The study was conducted in accordance with the Declaration of Helsinki.

2.2 | Antibodies

The primary and secondary antibodies used in this study are summarized in Table S1.

2.3 | Immunohistochemistry

Immunohistochemistry was performed using the ABC method with the VECTASTAIN Elite ABC Rabbit and Mouse IgG Kit (PK-6101 and PK-6102; Vector Laboratories), following the manufacturer's protocol. Three gynecologic oncologists (Ma.Ko., S.N., and Y.K.), each trained in pathological diagnosis, independently evaluated protein expression levels using a visual grading system based on staining intensity observed under a light microscope. For VRK1, VRK2, and cytochrome c oxidase subunit IV (COX IV), the H-score was used for quantification [31]. For Ki-67 and cleaved caspase-3, immunohistochemistry-positive and total cells were imaged at 400× magnification and counted using ImageJ software [32]. The proportion of positive cells was evaluated in three microscopic fields per lesion.

2.4 | Cell Lines and Two-Dimensional (2D) Cell Culture

One SCNEC cell line (HCSC-1), three SCC cell lines (CaSki, ME-180, and BOKU), and one AC cell line (HeLa) were purchased from the Japanese Collection of Research Bioresources Cell Bank (Osaka, Japan). Another SCNEC cell line (TC-YIK) was purchased from the RIKEN BioResource Research Center Cell

Bank (Ibaraki, Japan). Another SCC cell line (SiHa) was purchased from the American Type Culture Collection (Manassas, VA, USA). All media were supplemented with 10% fetal bovine serum, penicillin (100 IU/mL), and streptomycin (100 μg/mL). All cell lines were cytogenetically tested and authenticated using the short tandem repeat method, with the most recent validation performed in November 2024. All experiments were performed with mycoplasma-free cells.

2.5 | Short Hairpin RNA (shRNA)-Mediated Knockdown of *VRK1*

VRK1 shRNA (h) Lentiviral Particles (sc-106702-V) containing three target-specific constructs for knocking down *VRK1* (Table S2) and copGFP Control Lentiviral Particles (sc-10884) were purchased from Santa Cruz Biotechnology (Santa Cruz, CA, USA). To generate stable *VRK1* knockdown in HCSC-1 and TC-YIK cells, the cells were infected with *VRK1* shRNA or control lentiviral particles in the presence of polybrene (Santa Cruz Biotechnology, Santa Cruz, CA, USA) at a final concentration of 5 μg/mL in complete medium. Stable clones were selected in culture medium containing 4 μg/mL puromycin (Santa Cruz Biotechnology, California, USA) and subsequently expanded. The knockdown efficiency was determined using western blot analysis.

2.6 | Western Blot Analysis

Western blot analysis was performed using sodium dodecyl sulfate-polyacrylamide gel electrophoresis [33, 34]. Membranes were blocked with Bullet Blocking One for Western Blotting (Nacalai Tesque, Kyoto, Japan), then incubated sequentially with primary antibodies overnight at 4°C and secondary antibodies for 1 h at 20°C–25°C. Membranes were detected using chemiluminescence with Chemi-Lumi One Super (Nacalai Tesque, Kyoto, Japan) and imaged using a ChemiDoc MP Imaging System (Bio-Rad Laboratories, Hercules, CA, USA). Quantitative analysis of the western blot bands was conducted using Image Lab Software (Bio-Rad Laboratories, Hercules, CA, USA).

2.7 | 2D Cell Culture In Vitro Proliferation Assay

The WST-8 assay was performed using Cell Count Reagent SF (Nacalai Tesque, Kyoto, Japan) following the manufacturer's protocol. To assess the effect of VRK1 knockdown, 5000 cells were seeded into each well of a 96-well plate. After 96 h, the WST-8 solution was added to each well, and absorbance was measured at 450 nm using a Multiskan FC Microplate Photometer (Thermo Fisher Scientific Inc., Waltham, MA, USA). To assess the effect of hydrogen peroxide (H_2O_2) treatment, HCSC-1 and TC-YIK cells were seeded into 96-well plates (20,000 cells per well).

2.8 | Colony Formation Assay

Cells were plated in 12- or 24-well plates. The cell counts and incubation times according to the cell type are shown in Table S3. When the incubation time exceeded 4 days, the medium was changed every 4 days. The cells were fixed with methanol at room temperature for 5 min, then stained with crystal violet solution (0.5% w/v crystal violet in 25% methanol) at room temperature for 30 min for TC-YIK cells or 50 min for HCSC-1 cells. The plates were washed and allowed to dry overnight. Each plate was scanned using an Epson scanner (Epson WorkForce GT-1500, Nagano, Japan) and quantified using ImageJ software [32].

2.9 | 3D Cell Culture and Viability Assay

Cells were propagated as monolayers before 3D cell culture. HCSC-1 spheroids were formed using a low-attachment 96-well plate with 4000 cells per 100 μL of 2% Matrigel and cultured for 7 days. TC-YIK spheroids were formed using a scaffold-based method, with 500 cells in 10 μL Matrigel droplets suspended in 100 μL of culture medium and cultured for 7 days. Cell viability was analyzed using the CellTiter-Glo 3D assay (Promega, USA), and spheroids larger than 2500 μm^2 were counted using ImageJ [32].

2.10 | In Vivo Experiments

BALB/cAJcl-nu/nu mice were purchased from CLEA Japan Inc. (Tokyo, Japan). Seven-week-old female mice were subjected to unilateral dorsal subcutaneous implantation of VRK1 knockdown (shVRK1) HCSC-1 cells (5×10^6 cells) or control (shCont) HCSC-1 cells, and shVRK1 TC-YIK cells (2×10^7 cells) or shCont TC-YIK cells in 100 μL of phosphate-buffered saline mixed with 50 μL of Matrigel matrix (Corning, NY, USA). Tumor volumes were measured twice per week using the following formula: (tumor volume, mm^3) = (major axis, mm) × (minor axis, $mm)^2 \times 0.5$. The mice were monitored over time for changes in body mass. When the major axis of the maximum tumor exceeded 20 mm, all mice were sacrificed, and the tumor xenografts were resected.

2.11 | RNA-Sequencing (RNA-Seq) Analysis of Xenograft Tumors

Xenograft tumors from BALB/cAJcl-nu/nu mice were analyzed: shVRK1 HCSC-1, shVRK1 TC-YIK, and respective shCont groups ($n = 3$ per group). RNA was isolated using a RNeasy Mini Kit (QIAGEN, Venlo, Netherlands), and quality was assessed with an Agilent 2100 Bioanalyzer. Libraries were prepared using the TruSeq Stranded mRNA Library Kit (Illumina) and sequenced on the Illumina NovaSeq6000, generating 101 bp × 101 bp paired-end reads. Gene expression tables were generated from the FASTQ files using ikra (version 2.0.1), an RNA-seq pipeline developed for salmon [35]. RNA-seq analyses were conducted using R software (version 4.2.3). The DESeq2 package (version 1.38.3) was used to generate normalized counts and perform differential gene expression analyses. Gene set enrichment analysis (GSEA) was performed using the ClusterProfiler package (version 4.6.2). Gene lists from DESeq2 were converted to Entrez IDs and subjected to Gene Ontology (GO) via GSEA.

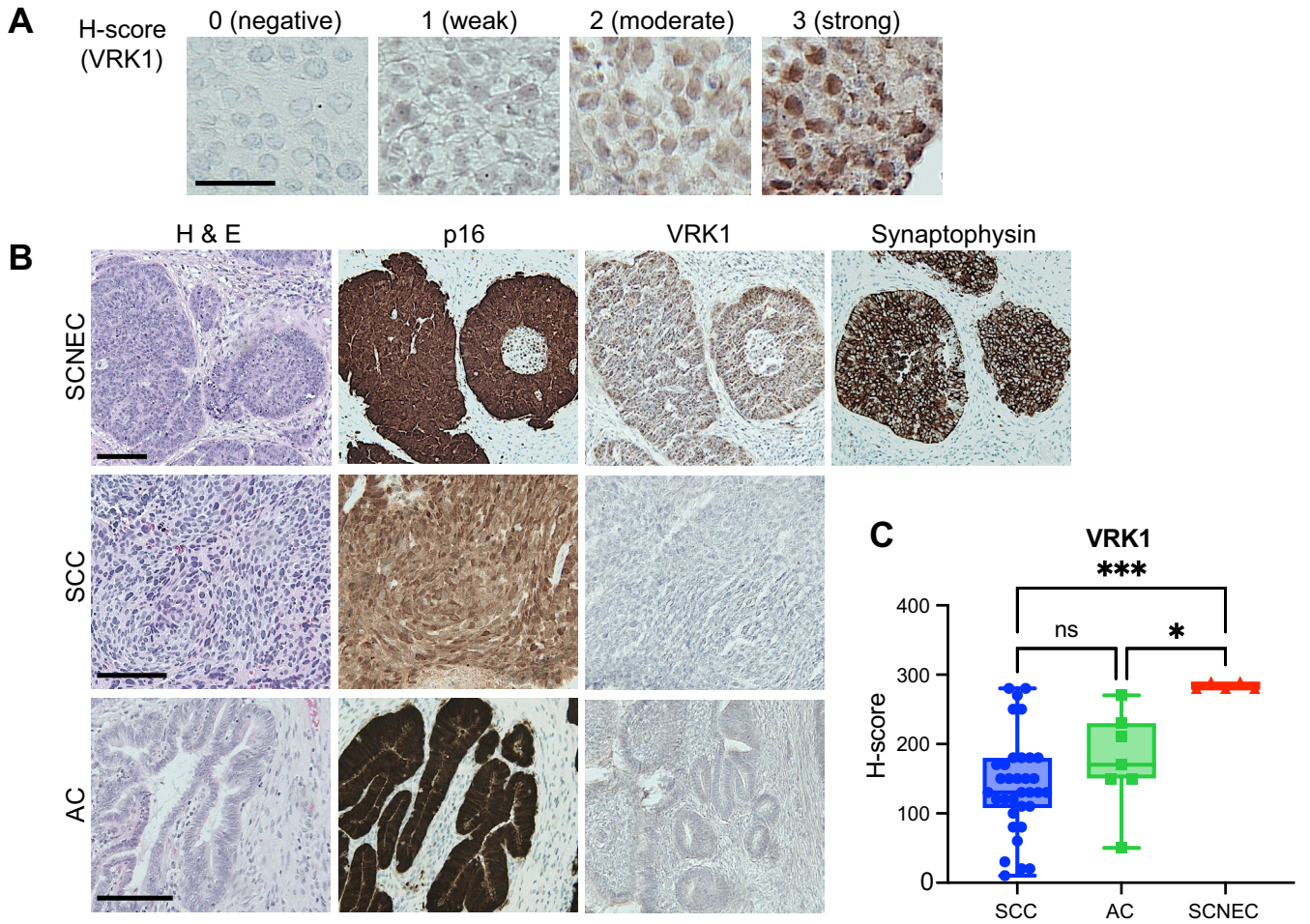

FIGURE 1 | VRK1 is highly expressed in SCNEC. (A) Representative images of VRK1 immunohistochemistry staining corresponding to H-scores of 0 (negative), 1 (weak), 2 (moderate), and 3 (strong) for SCC. Scale bars: 40 μm. (B) Representative images of H&E staining and VRK1 immunohistochemistry staining for SCNEC. Scale bars: 100 μm. (C) Box plots showing VRK1 H-scores across SCNEC, SCC, and AC patients. The centerlines in the boxplots indicate medians, and the box limits represent the minimum and maximum values. Statistical analysis was performed using one-way ANOVA followed by Tukey's multiple comparison test (C). ns, not significant; $*p < 0.05$; $***p < 0.001$.

2.12 | Analysis of Mitochondrial Membrane Potential

The mitochondrial membrane potential of HCSC-1 cells was analyzed using the MT-1 MitoMP Detection Kit (#MT13) (Dojindo Laboratories, Kumamoto, Japan) following the manufacturer's protocol. Cells were seeded at a density of 4×10^4 cells/well in 96-well plates and stained with Hoechst 33342 (5 μM; AAT Bioquest, CA, USA) to detect nuclei. Assessment in TC-YIK cells was technically challenging, as they are suspension cells and could not tolerate multiple washing steps.

2.13 | Statistical Analysis

Statistical analyses were performed using GraphPad Prism 10 (GraphPad Software, San Diego, CA, USA) and Microsoft Excel (Microsoft Corporation, Redmond, WA, USA). Significance was tested using a two-tailed Student's *t*-test for single comparisons, one-way analysis of variance followed by Tukey's multiple comparison test for continuous variables with multiple groups, and Pearson's chi-squared test for categorical variables with multiple groups. Experimental data are presented as the mean ± standard deviation, except for in vivo experiments, where the data are presented as mean ± standard error of the mean. Statistical significance was set at $p < 0.05$. In our figures, statistical significance is indicated as follows: $*p < 0.05$; $**p < 0.01$; $***p < 0.001$; $****p < 0.0001$; ns, not significant.

3 | Results

3.1 | VRK1 Is Highly Expressed in SCNEC Clinical Samples

To explore VRK1 expression across different histological types of cervical cancer, immunohistochemistry was performed on formalin-fixed paraffin-embedded clinical samples (Figure 1A). The study included five patients of SCNEC, 34 patients of SCC, and seven patients of AC (Table S4). Like SCC and AC, SCNEC is a human papillomavirus (HPV)-related cancer and exhibited positivity for p16 (Figure 1B). Furthermore, synaptophysin, a neuroendocrine marker, was positive in SCNEC. Quantitative evaluation of immunohistochemical staining based on chromogenic signal intensities revealed that VRK1 expression varied widely in SCC and AC, whereas it was uniformly high

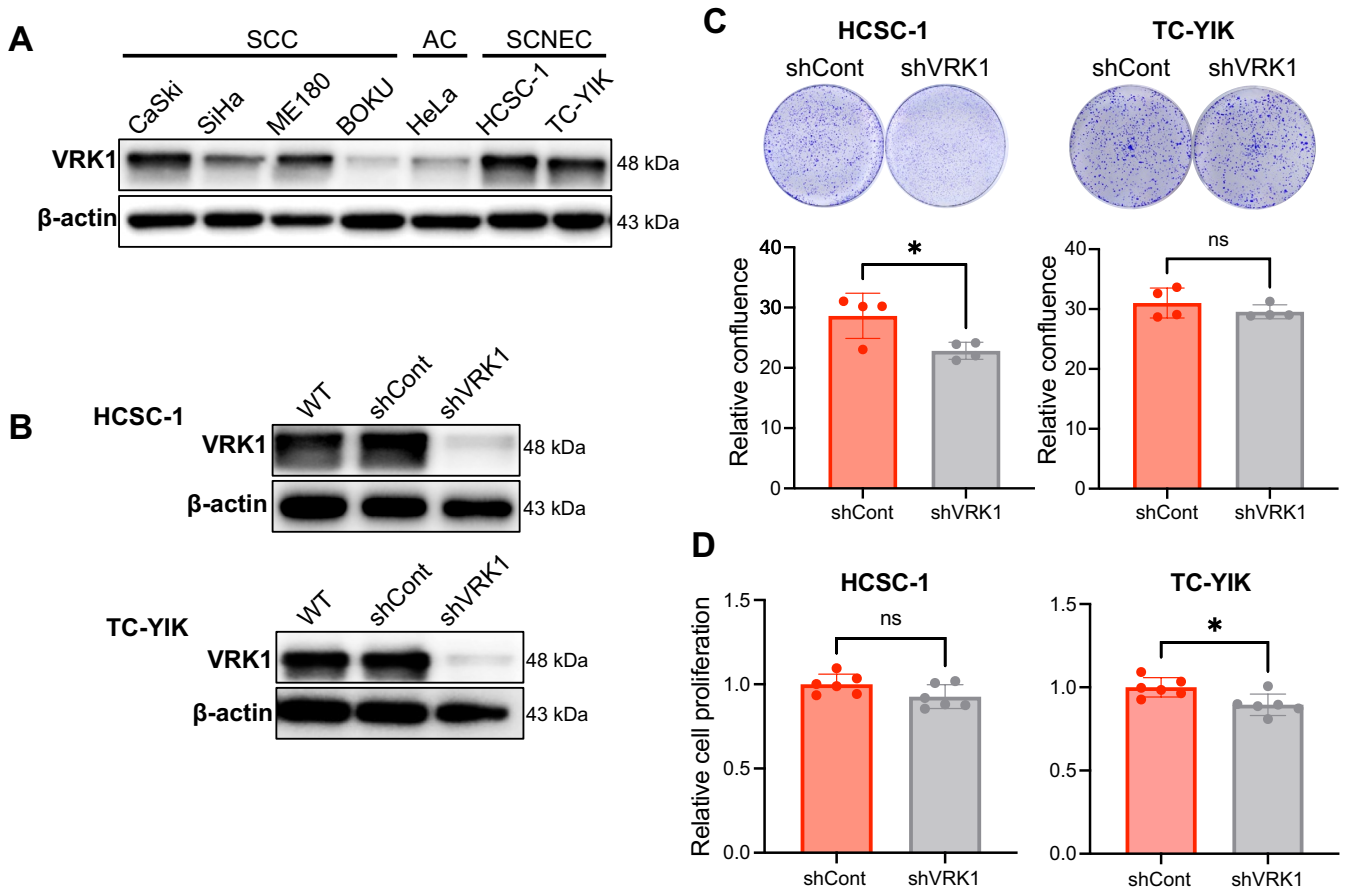

FIGURE 2 | VRK1 knockdown in SCNEC had a limited effect on proliferation in 2D cultures. (A) Western blot analysis detecting VRK1 expression in SCNEC (HCSC-1 and TC-YIK), SCC (CaSki, SiHa, ME180, and BOKU), and AC (HeLa). (B) Western blot analysis of VRK1 expression in HCSC-1 and TC-YIK cells. WT, wild-type; shCont, control; shVRK1, VRK1 knockdown. (C) Colony formation assay in 2D culture over 7 days comparing shCont and shVRK1 in HCSC-1 and TC-YIK cells ($n = 4$). (D) Proliferation assay in 2D culture over 96 h, comparing shCont and shVRK1 in HCSC-1 and TC-YIK cells ($n = 6$). Data are presented as the mean ± standard deviation (C and D). Statistical analysis was performed using two-tailed unpaired Student's *t*-tests (C and D). ns, not significant; $^*p < 0.05$.

across all SCNEC samples (SCNEC: mean = 284, range: 280–290; SCC: mean = 140, range: 10–280; AC: mean = 176, range: 50–270; SCNEC vs. SCC: $p < 0.001$, SCNEC vs. AC: $p < 0.05$) (Figure 1B,C). Additionally, RNA microarray data from patient-derived organoids available in GEO datasets were analyzed. Compared with the control AC sample (cerv51), all SCNEC samples ($n = 10$) showed higher VRK1 expression (Figure S1). These findings suggest that SCNEC consistently exhibits high VRK1 expression.

3.2 | Limited Effect of VRK1 Knockdown on SCNEC Proliferation in 2D Culture

We investigated the role of VRK1 in SCNEC proliferation in 2D culture. Similar to the clinical samples, VRK1 expression varied in SCC and AC cell lines, whereas both SCNEC cell lines, HCSC-1 and TC-YIK, consistently exhibited high VRK1 expression (Figure 2A). *VRK1* was knocked down using shRNA, and knockdown efficiency was validated using western blot analysis (Figure 2B).

VRK1 knockdown resulted in a slight but significant reduction in colony formation in HCSC-1 cells compared with that in the control, while no significant difference was observed in TC-YIK cells (Figure 2C). Conversely, WST-8 assays showed that cell proliferation was slightly but significantly suppressed in TC-YIK cells, but not in HCSC-1 cells following VRK1 knockdown (Figure 2D). These findings suggested that VRK1 knockdown in SCNEC had a limited effect on the proliferation in 2D cultures.

VRK1 regulates and stabilizes p53 [18, 36]. Carcinomas associated with high-risk HPV infection exhibit functional loss of p53 due to the viral E6 protein, which promotes p53 degradation by recruiting the cellular ubiquitin ligase E6AP [37]. As a result, these carcinomas display low levels of p53 expression. All cell lines used in this study were reported positive for HPV infection (Table S5). Additionally, *TP53* mutation in TC-YIK cells (exon 6, c.652_654del, p.V218del) has been previously reported [38]. Based on these findings, we evaluated p53 protein expression in SCNEC cell lines by western blot analysis. Wild-type p53 protein expression was not detected in TC-YIK cells (Figure S2A). In HCSC-1 cells, the *TP53* mutation status is unknown, and only a faint p53 band was observed (Figure S2A). Notably, VRK1 knockdown in HCSC-1 cells did not alter p53 protein levels (Figure S2B). These results suggest that the effects of VRK1 knockdown on SCNEC cell proliferation are likely independent of p53 stabilization.

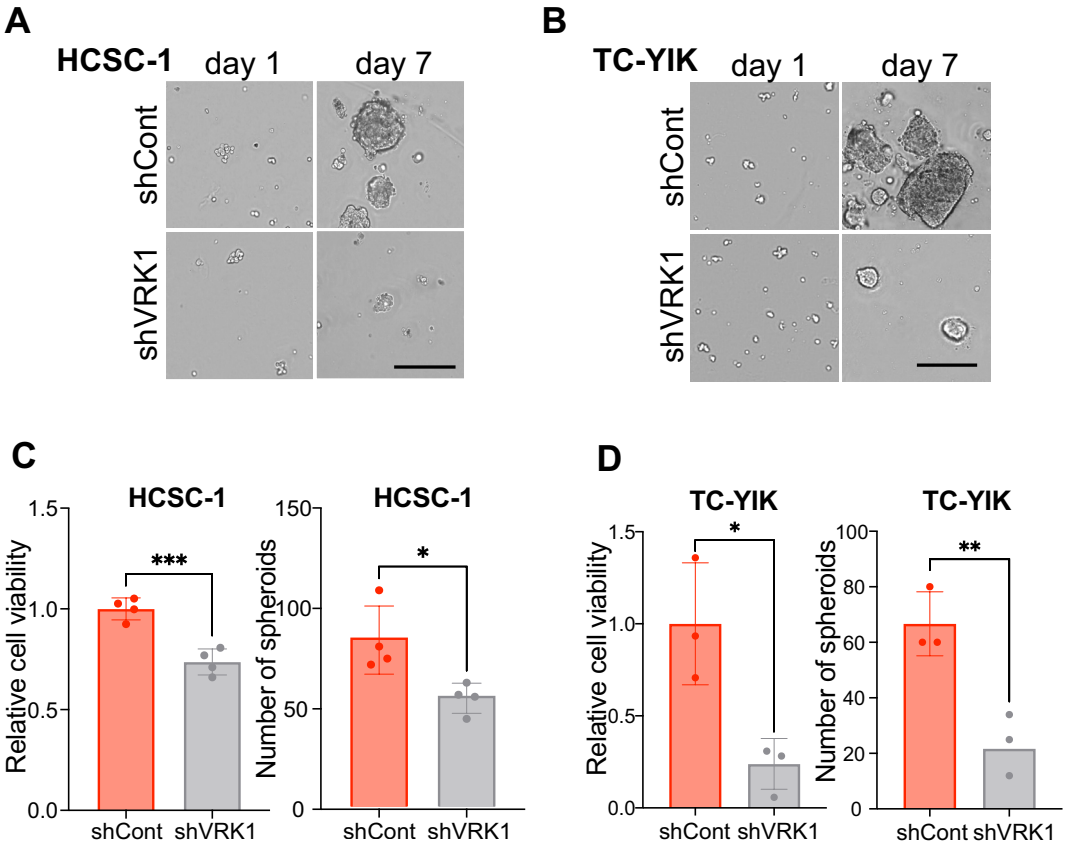

FIGURE 3 | VRK1 knockdown in SCNEC significantly suppressed proliferation in 3D cultures. (A and B) Representative 3D culture images comparing shVRK1 and shCont on days 1 and 7. (A) HCSC-1 and (B) TC-YIK cells. Scale bars: 200 μm. (C and D) CellTiter-Glo 3D cell viability assays and spheroid counts (> 2500 μm^2) over 7 days. Comparison of shCont and shVRK1 in HCSC-1 (C, $n = 4$) and TC-YIK (D, $n = 3$). Data are presented as mean ± standard deviation in C and D. Statistical analyses were performed using two-tailed Student's *t*-tests (C and D). $^*p < 0.05$; $^{**}p < 0.01$; $^{***}p < 0.001$.

3.3 | VRK1 Knockdown in SCNEC Significantly Suppresses Tumor Growth in 3D Cultures and In Vivo

We explored the effects of VRK1 on tumor growth in both 3D cultures and in vivo mouse xenograft models. Unlike traditional 2D monolayer cultures, 3D cultures allow cells to interact with their surroundings in all directions [39]. VRK1 knockdown in SCNEC cells significantly inhibited tumor growth in 3D cultures, as opposed to the limited effects observed in 2D cultures (Figure 3A–D). Similar results were observed in the in vivo subcutaneous xenograft mouse model (Figure 4A–D; Figure S3; Figure S4). Maintenance of VRK1 knockdown during the observation period was confirmed via western blot analysis (Figure S4).

We further evaluated the expression of Ki-67, a marker of cell proliferation, and cleaved caspase-3, a marker of apoptosis, in xenograft tumors using immunohistochemical staining. The proportion of Ki-67-positive cells was significantly lower in shVRK1 tumors compared with that in shCont tumors (HCSC-1: Figure 4E; TC-YIK: Figure S5A). In addition, the proportion of cleaved caspase-3-positive cells was significantly higher in shVRK1 tumors compared with that in shCont tumors (HCSC-1: Figure 4F; TC-YIK: Figure S5B). These findings suggest that VRK1 knockdown exerts a significant antitumor effect in vivo by inhibiting cell proliferation and promoting apoptosis, underscoring its potential as a novel therapeutic target for SCNEC.

3.4 | VRK1 Is Associated With the Mitochondrial Pathway In Vivo

To investigate the role of VRK1, we performed GSEA of shCont versus shVRK1 RNA-seq data from subcutaneous tumors derived from SCNEC cell lines in mice (Figure 5A). GSEA of tumors derived from HCSC-1 cells revealed that mitochondrial translation and gene expression were the most prominently suppressed pathways in shVRK1 tumors, ranking above previously reported pathways, such as those related to the cell cycle and DNA replication (Figure 5B; Table S6) [17, 18, 26–27]. The pathways associated with ATP generation via mitochondria were also significantly suppressed in shVRK1 tumors (Figure S6A; Table S6) [40, 41]. These findings were consistent with GSEA results of shCont versus shVRK1 tumors derived from another SCNEC cell line, TC-YIK (Figure S6B; Table S7).

Immunohistochemistry analysis of mouse xenograft subcutaneous tumors further confirmed that the expression of COX IV was significantly decreased in shVRK1 tumors (Figure S7; HCSC-1: Figure 5C,D; TC-YIK: Figure S8). COX IV is a subunit of cytochrome c oxidase (COX), the terminal enzyme complex of the mitochondrial respiratory chain, and it is encoded by nuclear

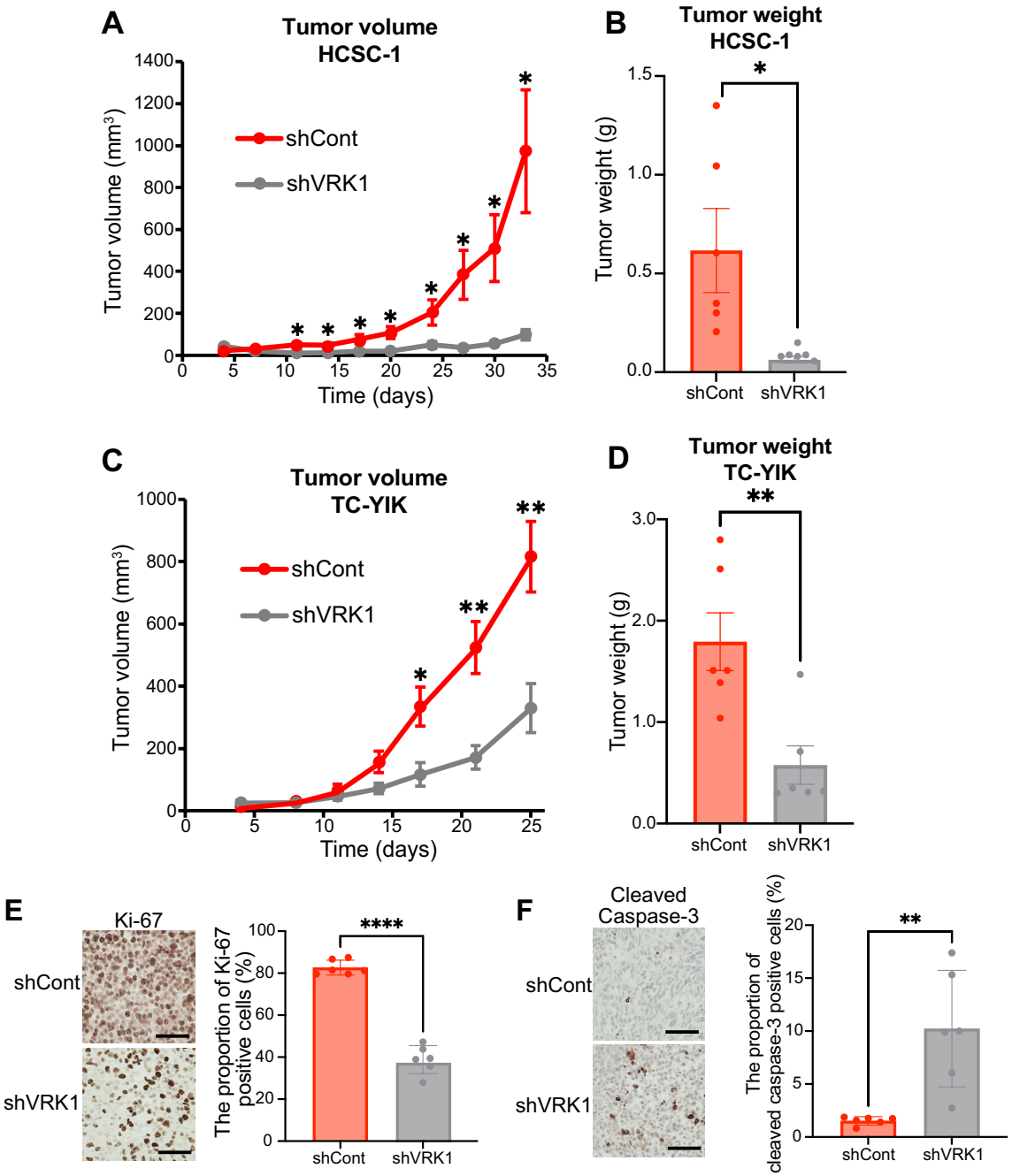

FIGURE 4 | VRK1 knockdown in SCNEC significantly suppresses tumor growth in vivo. (A and B) Tumor volumes and weights in HCSC-1 xenografts ($n = 6$), measured sequentially and post-euthanasia. (A) Tumor volumes and (B) tumor weights, comparing shCont and shVRK1. (C and D) Tumor volumes and weights in TC-YIK xenografts ($n = 6$). (C) Tumor volumes and (D) tumor weights, comparing shCont and shVRK1. (E and F) (E) Ki-67 and (F) cleaved caspase-3 immunohistochemistry staining in HCSC-1 xenografts, with bar plots showing the proportion of positive cells. Scale bars: 50 μm. Comparison of shCont versus shVRK1 ($n = 6$). Data are presented as mean ± standard deviation in E and F, and mean ± standard error of mean in A–D. Statistical analyses were performed using two-tailed Student's *t*-tests (A–F). *$p < 0.05$; **$p < 0.01$; ****$p < 0.0001$.

DNA [42]. Taken together, these results suggest that VRK1 is associated with mitochondrial activity in SCNEC.

3.5 | VRK1 Regulates the Mitochondrial Stress Response Under Oxidative Stress

Given the differences observed in the effects of VRK1 knockdown on cell proliferation between 2D and 3D cultures or in vivo conditions, we hypothesized that VRK1 might be involved in regulating responses to specific external stimuli characteristic of 3D and in vivo environments (Figures 2–4). Indeed, the GSEA revealed that VRK1 was associated with the regulation of responses to external stimuli (Figure 5B; Figure S9; Tables S6 and S7). To explore this further, we examined changes in cell proliferation following VRK1 knockdown under hypoxia, nutrient deprivation, and exposure to reactive oxygen species (ROS), all of which are typically encountered

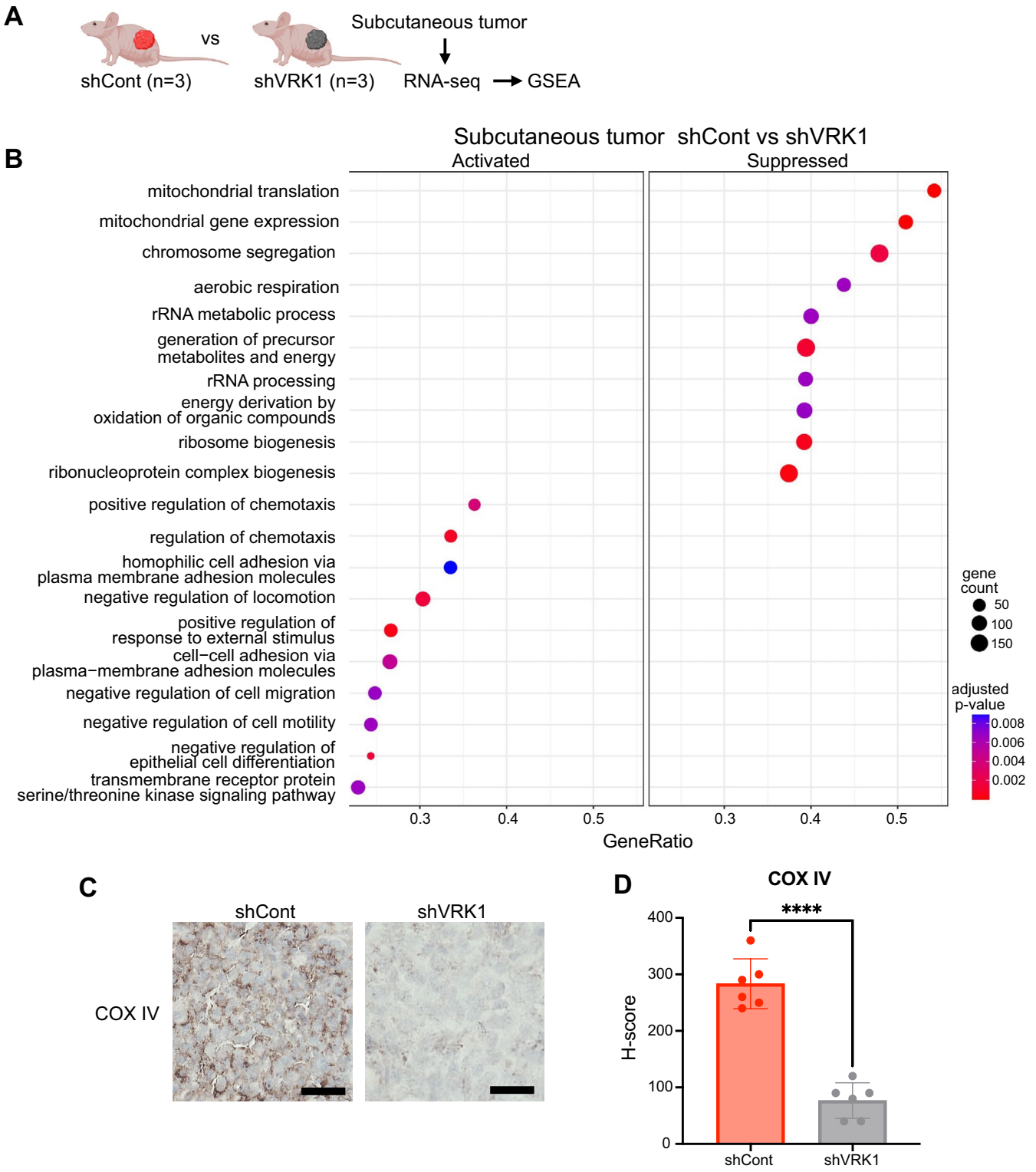

FIGURE 5 | VRK1 is associated with mitochondrial pathways in vivo. (A) Schematic outline of the experimental procedure for GSEA of RNA-seq analysis from subcutaneous tumors. (B) Dot plot showing enriched pathways ranked by gene ratio in tumors derived from shVRK1 cells compared with shCont cells, based on GSEA of RNA-seq data from mouse xenograft tumors derived from HCSC-1 cells. Dot sizes represent the gene count, while dot colors represent the adjusted *p*-value. (C) Representative images of COX IV immunohistochemistry staining for mouse xenograft tumors derived from HCSC-1. Scale bars: 20 μm. (D) Bar plot showing COX IV H-scores to compare shCont versus shVRK1 ($n = 6$). Data are presented as mean ± standard deviation in D. Statistical analysis was performed using a two-tailed Student's *t*-tests (D). ****$p < 0.0001$.

in tumors in vivo [30]. Conditions with exposure to ROS were generated using H_2O_2. Notably, nutrient deprivation and hypoxic conditions did not alter the relationship between VRK1 expression and cell proliferation (Figures S10 and S11). In contrast, VRK1 knockdown caused a dose-dependent increase in sensitivity to H_2O_2 and a decline in colony formation

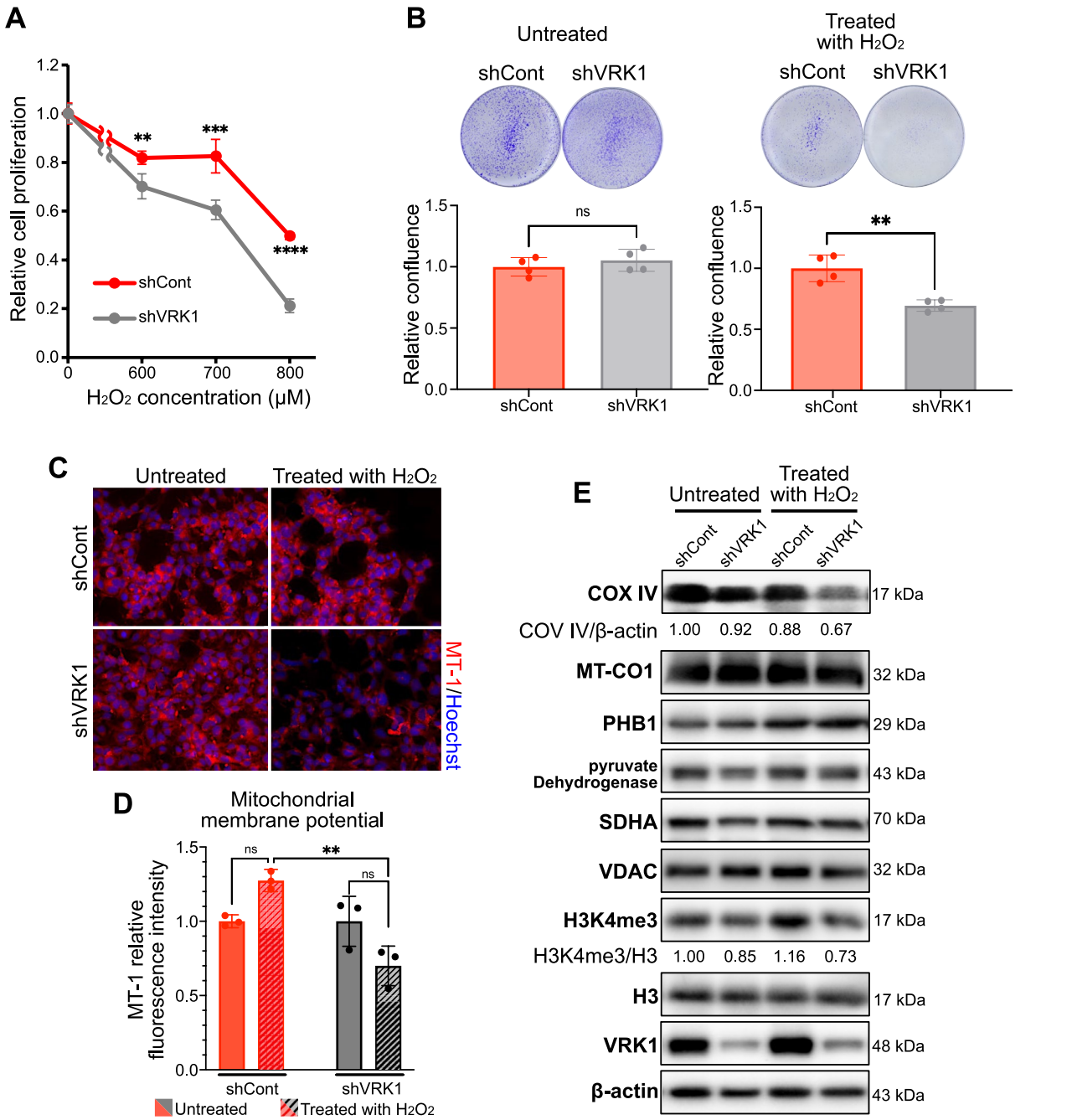

FIGURE 6 | VRK1 is associated with sensitivity to oxidative stress via mitochondrial function. (A) Proliferation assay of HCSC-1 cells after treatment with 0, 600, 700, and 800 μM H_2O_2 for 48 h in 2D cultures. Comparison of shCont versus shVRK1 ($n = 6$). (B) Colony formation assay of HCSC-1 cells after treatment with or without 800 μM H_2O_2 for 48 h in 2D cultures. Comparison of shCont and shVRK1 cells ($n = 4$). (C and D) HCSC-1 cells were stained with MT-1 to measure mitochondrial membrane potential. Representative fluorescence images (C) and quantitative analysis of the chromogenic signal intensities (D). Cells were treated with or without 600 μM H_2O_2 for 24 h in 2D culture. Comparison of shCont versus shVRK1 ($n = 3$). (E) Western blot analysis detecting the expression levels of mitochondria-related proteins and the levels of epigenetic histone marks in HCSC-1 cells treated with or without 800 μM H_2O_2 for 6 h. Data are represented as the mean ± standard deviation. Statistical analyses were performed using two-tailed Student's *t*-tests (A and B) and one-way ANOVA followed by Tukey's multiple comparison test (D). ns, not significant; $^{**}p < 0.01$; $^{***}p < 0.001$; $^{****}p < 0.0001$.

following H_2O_2 treatment in VRK1-knockdown cells (HCSC-1: Figure 6A,B; TC-YIK: Figure S12). These findings suggest that VRK1 knockdown is associated with increased vulnerability of SCNEC to ROS-induced stress.

We evaluated changes in mitochondrial function following VRK1 knockdown under ROS exposure in HCSC-1 cells. A significant decrease in mitochondrial membrane potential, an indicator of mitochondrial integrity, was observed in VRK1-knockdown SCNEC cells after H_2O_2 treatment (Figure 6C,D). Additionally, COX IV expression was reduced by VRK1 knockdown and further decreased in VRK1-knockdown cells treated with H_2O_2 (HCSC-1: Figure 6E; TC-YIK: Figure S13). In contrast, the expression of MT-CO1, a subunit of COX encoded

by mitochondrial DNA, as well as other mitochondria-related proteins, remained unchanged (HCSC-1: Figure 6E; TC-YIK: Figure S13).

Evaluation of the subcellular localization of VRK1 revealed that it was predominantly localized in the nucleus, with partial presence in the cytoplasm (Figure S14). However, colocalization with mitochondria was not observed (Figure S14). In addition, VRK1 suppressed the levels of H3K4me3, an epigenetic histone posttranslational modification and an activating mark associated with gene promoters and active transcription (HCSC-1: Figure 6E; TC-YIK: Figure S13).

These results suggest that VRK1 plays an important role in regulating the mitochondrial stress response under oxidative stress. This effect may be mediated by epigenetic histone posttranslational modification induced by VRK1, resulting in the indirect suppression of COX IV expression.

4 | Discussion

As the outcomes of conventional SCNEC treatments remain unsatisfactory, the development of specialized pharmacological therapies is warranted [2, 4, 5, 7–9]. In light of this, we focused on VRK1, identified in our previous proteomic analysis using patient-derived organoids [11]. Notably, SCNEC is characterized by high VRK1 expression, and VRK1 knockdown significantly suppressed tumor growth in both 3D culture and in vivo models. Mechanistically, VRK1 was indirectly involved in mitochondrial function in response to oxidative stress during SCNEC proliferation. Based on its unique molecular characteristics, we propose VRK1 as a novel therapeutic target for SCNEC.

We demonstrated that VRK1 expression is consistently high in SCNEC, in contrast to SCC and AC. Regarding AC, a previous study reported no significant difference in VRK1 protein expression between SCNEC and mucinous adenocarcinoma of the cervix [11]. The discrepancy between our findings and a prior report is likely attributable to the following methodological differences: (i) the primary antibodies used for immunohistochemistry, (ii) the scoring method employed, and (iii) the analyzed case cohorts [31]. While the previous study evaluated only the area fraction of positive cells for scoring, we adopted the H-score method, which quantitatively integrates both staining intensity and the proportion of positive cells [31].

In our study, the effect of VRK1 knockdown on SCNEC proliferation and tumor growth differed between traditional 2D cultures and 3D cultures or in vivo conditions. Traditional 2D monolayer cell culture models lack the tumor microenvironment [39, 43]. In contrast, 3D cultures promote these interactions and more accurately recapitulate the characteristics of tumor cells in vivo, such as nutrient and oxygen concentration gradients [39, 43]. Our results revealed that ROS exposure, arising from the combined effects of the tumor microenvironment and high-energy metabolism of the tumor itself, which are required for uncontrolled growth and spread, influenced the tumor growth-inhibitory effect of VRK1 knockdown in a dose-dependent manner [41, 44].

VRK1 regulates chromatin remodeling indirectly by modulating epigenetic enzymes responsible for histone posttranslational modifications [29]. VRK1 depletion has been reported to downregulate activating histone marks such as H3K4me3 and upregulate repressive marks including H3K9me3 and H3K27me3 [29]. Consistent with these findings, we demonstrated that VRK1 knockdown induces H3K4me3 downregulation in SCNEC cell lines. VRK1 is also essential for the DNA damage response, and its loss alters both the histone epigenetic pattern and nuclear phosphoproteome pathways under oxidative stress [30]. While a previous study reported that VRK1 depletion altered the pattern of histone epigenetic modifications induced by oxidative stress and increased H3K4me3 levels, our findings demonstrate that VRK1 knockdown reduces H3K4me3 levels under the same conditions [30]. This difference may reflect differences in the cellular context, such as the state of p53 and the temporal dynamics of chromatin modification. The degree of ROS exposure may also be a cause of these differences. Since VRK1 functions within a complex regulatory network involving histone-modifying enzymes, its effect on H3K4me3 is likely context-dependent and influenced by the intensity of oxidative stress [30]. Based on our findings, we hypothesize that the downregulation of H3K4me3, a transcriptionally activating histone mark, may suppress COX IV expression and thereby impair mitochondrial function. However, further investigation is required to determine whether this effect is direct.

The results of this study suggest that VRK1 is associated with mitochondrial function. Mitochondria are not only essential organelles for energy production but also play various roles in cellular stress responses [45]. Mitochondrial dysfunction caused by cytotoxic stress triggers processes such as apoptosis, necroptosis, and ferroptosis [41, 45]. In this context, our immunohistochemical analysis of mouse xenograft tumors revealed an increase in cleaved caspase-3-positive cells following VRK1 knockdown, supporting its involvement in apoptosis.

Recently, VRK1 has been identified as a synthetic lethal target in VRK2-deficient nervous system cancers [26, 27, 46]. We identified SCNEC as a distinct tumor type characterized by low VRK2 expression (Figure S15). VRK1 and VRK2 are paralogous genes that may exhibit functional redundancy [46]. These findings suggest that the potential synthetic lethality between VRK1 and VRK2 could have therapeutic relevance for SCNEC, warranting further investigation. Importantly, no normal tissue exhibits a VRK1-VRK2 expression pattern similar to SCNEC, VRK1-high, and VRK2-low, which could potentially mitigate adverse effects associated with VRK1 inhibition (Figure S16).

In conclusion, the current study demonstrates that SCNEC is characterized by high VRK1 expression and low VRK2 expression. Notably, VRK1 knockdown suppresses tumor growth via indirect mitochondrial dysfunction. Our findings suggest that VRK1 is a promising therapeutic target for SCNEC.

Author Contributions

Mariya Kobayashi: conceptualization, data curation, formal analysis, investigation, methodology, validation, visualization, writing – original

draft, writing – review and editing. **Satoshi Nakagawa:** conceptualization, funding acquisition, investigation, methodology, project administration, resources, validation, writing – original draft, writing – review and editing. **Yuji Kamei:** data curation, formal analysis, software, validation, visualization, writing – review and editing. **Mizuki Kanda:** investigation, validation, writing – review and editing. **Tatsuo Masuda:** formal analysis, software, writing – review and editing. **Mamoru Kakuda:** resources, writing – review and editing. **Kosuke Hiramatsu:** funding acquisition. **Tadashi Iwamiya:** resources, writing – review and editing. **Tomomi Egawa-Takata:** writing – review and editing. **Shinya Matsuzaki:** funding acquisition, writing – review and editing. **Hiroyuki Uematsu:** resources, writing – review and editing. **Kunishige Onuma:** resources, writing – review and editing. **Masahiro Inoue:** resources, supervision, writing – review and editing. **Yutaka Ueda:** funding acquisition, project administration, supervision, writing – review and editing. **Tadashi Kimura:** writing – review and editing. **Michiko Kodama:** writing – review and editing. **Yusuke Ishii:** writing – review and editing.

Acknowledgments

We are grateful to the members of the Department of Obstetrics and Gynecology, Pathology Laboratory, Graduate School of Medicine, Osaka University, for the valuable discussions and suggestions throughout this project. We also thank Hazuki Abe and Kanako Sakiyama for their technical and administrative assistance in the preparation of this manuscript. Additionally, we would like to acknowledge Editage (https://www.editage.jp/) for their English language editing.

Ethics Statement

Approval of the research protocol by an Institutional Review Board: This study was approved by the Osaka University Research Ethics Committee (Approval Nos. 15262 and 24461). Registry and the Registration No. of the study/trial: N/A. Informed Consent: All patients provided written consent. Animal Studies: All animal experiments were carried out according to the Institutional Ethical Guidelines for Animal Experimentation at Osaka University. Efforts were made to minimize suffering and to use the minimal number of animals necessary to achieve reliable scientific results.

Conflicts of Interest

H.U., K.O., and M.I. belong to the Department of Clinical Bio-resource Research and Development at Kyoto University, which is sponsored by KBBM Inc. M.I. is an editorial board member of *Cancer Science*. The other authors declare no conflicts of interest.

Data Availability Statement

The data generated in this study is publicly available in the GEO under accession number GSE281857. The data analyzed in this study were obtained from the GSE164329 and GSE285993 GEO datasets, as well as the HPA public database [47, 48]. All other raw data are available upon request from the corresponding author.

References

1. J. Ferlay, M. Ervik, F. Lam, et al., "Global Cancer Observatory: Cancer Today (Version 1.1)," Lyon, France: International Agency for Research on Cancer (2025), https://gco.iarc.who.int/today.

2. M. Kobayashi, S. Nakagawa, T. Masuda, et al., "Clinical and Pathological Characteristics and Outcomes of Small Cell Neuroendocrine Carcinoma of the Uterine Cervix," *International Journal of Gynecological Cancer* 35 (2025): 102011.

3. American Cancer Society, "Survival Rates for Cervical Cancer," accessed January 26, 2025, https://www.cancer.org/cancer/types/cervical-cancer/detection-diagnosis-staging/survival.html.

4. J. G. Cohen, D. S. Kapp, J. Y. Shin, et al., "Small Cell Carcinoma of the Cervix: Treatment and Survival Outcomes of 188 Patients," *American Journal of Obstetrics and Gynecology* 203, no. 4 (2010): 347.e1–347.e6.

5. M. Seino, S. Nagase, T. Ohta, et al., "Impact of Adjuvant Chemotherapy on the Overall Survival of Patients With Resectable Bulky Small Cell Neuroendocrine Cervical Cancer: A JSGO-JSOG Joint Study," *Journal of Gynecologic Oncology* 34, no. 1 (2023): e4.

6. Y. Ito, I. Miyashiro, H. Ito, et al., "Long-Term Survival and Conditional Survival of Cancer Patients in Japan Using Population-Based Cancer Registry Data," *Cancer Science* 105, no. 11 (2014): 1480–1486.

7. G. Salvo, L. A. Meyer, N. R. Gonzales, M. Frumovitz, and R. T. Hillman, "Neuroendocrine Cervical Carcinomas: Genomic Insights, Controversies in Treatment Strategies, and Future Directions: A NeCTuR Study," *International Journal of Gynecological Cancer* 35, no. 3 (2025): 101639.

8. A. Chao, R. C. Wu, C. Y. Lin, T. C. Chang, and C. H. Lai, "Small Cell Neuroendocrine Carcinoma of the Cervix: From Molecular Basis to Therapeutic Advances," *Biomedical Journal* 46, no. 5 (2023): 100633.

9. T. Chu, Y. Meng, P. Wu, et al., "The Prognosis of Patients With Small Cell Carcinoma of the Cervix: A Retrospective Study of the SEER Database and a Chinese Multicentre Registry," *Lancet Oncology* 24, no. 6 (2023): 701–708.

10. National Comprehensive Cancer Network, "NCCN Clinical Practice Guidelines in Oncology (NCCN Guidelines): Cervical Cancer, Version 4.2024," accessed January 26, 2025, https://www.nccn.org/professionals/physician_gls/pdf/cervical.pdf.

11. T. Egawa-Takata, K. Yoshino, K. Hiramatsu, et al., "Small Cell Carcinomas of the Uterine Cervix and Lung: Proteomics Reveals Similar Protein Expression Profiles," *International Journal of Gynecological Cancer* 28, no. 9 (2018): 1751–1757.

12. B. Pan, S. Yan, L. Yuan, et al., "Multiomics Sequencing and Immune Microenvironment Characteristics Define Three Subtypes of Small Cell Neuroendocrine Carcinoma of the Cervix," *Journal of Pathology* 263, no. 3 (2024): 372–385.

13. F. Xu, J. Ma, H. Yi, et al., "Clinicopathological Aspects of Small Cell Neuroendocrine Carcinoma of the Uterine Cervix: A Multicenter Retrospective Study and Meta-Analysis," *Cellular Physiology and Biochemistry* 50, no. 3 (2018): 1113–1122.

14. J. George, J. S. Lim, S. J. Jang, et al., "Comprehensive Genomic Profiles of Small Cell Lung Cancer," *Nature* 524, no. 7563 (2015): 47–53.

15. R. N. Eskander, J. Elvin, L. Gay, J. S. Ross, V. A. Miller, and R. Kurzrock, "Unique Genomic Landscape of High-Grade Neuroendocrine Cervical Carcinoma: Implications for Rethinking Current Treatment Paradigms," *JCO Precision Oncology* 4 (2020): PO.19.00248.

16. C. Johansson and S. Schwartz, "Regulation of Human Papillomavirus Gene Expression by Splicing and Polyadenylation," *Nature Reviews Microbiology* 11 (2013): 239–251.

17. I. Campillo-Marcos and P. A. Lazo, "Implication of the VRK1 Chromatin Kinase in the Signaling Responses to DNA Damage: A Therapeutic Target?," *Cellular and Molecular Life Sciences* 75, no. 13 (2018): 2375–2388.

18. I. Campillo-Marcos, R. García-González, E. Navarro-Carrasco, and P. A. Lazo, "The Human VRK1 Chromatin Kinase in Cancer Biology," *Cancer Letters* 503 (2021): 117–128.

19. D. Chen, W. Zhou, J. Chen, and J. Wang, "Comprehensively Prognostic and Immunological Analysis of VRK Serine/Threonine Kinase 1 in Pan-Cancer and Identification in Hepatocellular Carcinoma," *Aging (Albany NY)* 15, no. 24 (2023): 15504–15524.

20. J. Li, T. Wang, L. Pei, et al., "Expression of VRK1 and the Downstream Gene BANF1 in Esophageal Cancer," *Biomedicine & Pharmacotherapy* 89 (2017): 1086–1091.

21. W. Huang, X. Cui, Y. Chen, et al., "High VRK1 Expression Contributes to Cell Proliferation and Survival in Hepatocellular Carcinoma," *Pathology, Research and Practice* 212, no. 3 (2016): 171–178.

22. A. Colmenero-Repiso, M. A. Gómez-Muñoz, I. Rodríguez-Prieto, et al., "Identification of vrk1 as a New Neuroblastoma Tumor Progression Marker Regulating Cell Proliferation," *Cancers (Basel)* 12, no. 11 (2020): 3465.

23. A. M. Mon, A. Craig MacKinnon, and P. Traktman, "Overexpression of the VRK1 Kinase, Which Is Associated With Breast Cancer, Induces a Mesenchymal to Epithelial Transition in Mammary Epithelial Cells," *PLoS One* 13, no. 9 (2018): e0203397.

24. J. Wu, T. Li, H. Ji, Z. Chen, and B. Zhai, "VRK1 Predicts Poor Prognosis and Promotes Bladder Cancer Growth and Metastasis In Vitro and In Vivo," *Frontiers in Pharmacology* 13 (2022): 874235.

25. X. He, G. Zai, L. Zhou, S. Chen, and G. Wang, "Identification of VRK1 as a Novel Potential Biomarker for Prognosis and Immunotherapy in Hepatocellular Carcinoma," *Journal of Inflammation Research* 17 (2024): 1671–1683.

26. J. A. Shields, S. R. Meier, M. Bandi, et al., "VRK1 Is a Synthetic-Lethal Target in VRK2-Deficient Glioblastoma," *Cancer Research* 82, no. 21 (2022): 4044–4057.

27. J. So, N. W. Mabe, B. Englinger, et al., "VRK1 as a Synthetic Lethal Target in VRK2 Promoter-Methylated Cancers of the Nervous System," *JCI Insight* 7, no. 19 (2022): e158755.

28. R. A. M. Serafim, F. H. De Souza Gama, L. A. Dutra, et al., "Development of Pyridine-Based Inhibitors for the Human Vaccinia-Related Kinases 1 and 2," *ACS Medicinal Chemistry Letters* 10 (2019): 1266–1271.

29. E. Monte-Serrano, P. Morejón-García, I. Campillo-Marcos, A. Campos-Díaz, E. Navarro-Carrasco, and P. A. Lazo, "The Pattern of Histone H3 Epigenetic Posttranslational Modifications Is Regulated by the VRK1 Chromatin Kinase," *Epigenetics & Chromatin* 16 (2023): 18.

30. E. Navarro-Carrasco, E. Monte-Serrano, A. Campos-Díaz, et al., "VRK1 Regulates Sensitivity to Oxidative Stress by Altering Histone Epigenetic Modifications and the Nuclear Phosphoproteome in Tumor Cells," *International Journal of Molecular Sciences* 25 (2024): 4874.

31. Z. Wen, D. Luo, S. Wang, et al., "Deep Learning–Based H-Score Quantification of Immunohistochemistry-Stained Images," *Modern Pathology* 37 (2024): 100398.

32. C. A. Schneider, W. S. Rasband, and K. W. Eliceiri, "NIH Image to ImageJ: 25 Years of Image Analysis," *Nature Methods* 9, no. 7 (2012): 671–675.

33. S. Nakagawa, S. Serada, R. Kakubari, et al., "Intratumoral Delivery of an Adenoviral Vector Carrying the SOCS-1 Gene Enhances T-Cell–Mediated Antitumor Immunity by Suppressing PD-L1," *Molecular Cancer Therapeutics* 17, no. 9 (2018): 1941–1950.

34. S. Matsuzaki, T. Enomoto, S. Serada, et al., "Annexin A4-Conferred Platinum Resistance Is Mediated by the Copper Transporter ATP7A," *International Journal of Cancer* 134 (2014): 1796–1809.

35. Y. Hiraoka, K. Yamada, R. Yamsasaki, et al., "yyoshiaki/ikra: Ikra v2.0," accessed November 16, 2024, https://doi.org/10.5281/zenodo.5541399.

36. F. M. Vega, A. Sevilla, and P. A. Lazo, "p53 Stabilization and Accumulation Induced by Human Vaccinia-Related Kinase 1," *Molecular and Cellular Biology* 24 (2004): 10366–10380.

37. L. M. Wootton and E. L. Morgan, "Ubiquitin and Ubiquitin-Like Proteins in HPV-Driven Carcinogenesis," *Oncogene* 44 (2025): 713–723.

38. "The TP53 Database Webpage," accessed Jun 15, 2025, https://tp53.cancer.gov/.

39. Y. M. Salinas-Vera, J. Valdés, Y. Pérez-Navarro, et al., "Three-Dimensional 3D Culture Models in Gynecological and Breast Cancer Research," *Frontiers in Oncology* 12 (2022): 826113.

40. I. S. Song, H. K. Kim, S. H. Jeong, et al., "Mitochondrial Peroxiredoxin III Is a Potential Target for Cancer Therapy," *International Journal of Molecular Sciences* 12, no. 10 (2011): 7163–7185.

41. P. E. Porporato, N. Filigheddu, J. M. B. S. Pedro, G. Kroemer, and L. Galluzzi, "Mitochondrial Metabolism and Cancer," *Cell Research* 28, no. 3 (2018): 265–280.

42. B. Kadenbach and M. Hüttemann, "The Subunit Composition and Function of Mammalian Cytochrome c Oxidase," *Mitochondrion* 24 (2015): 64–76.

43. S. Nath and G. R. Devi, "Three-Dimensional Culture Systems in Cancer Research: Focus on Tumor Spheroid Model," *Pharmacology & Therapeutics* 163 (2016): 94–108.

44. M. Azmanova and A. Pitto-Barry, "Oxidative Stress in Cancer Therapy: Friend or Enemy?," *Chembiochem* 23, no. 10 (2022): e202100641.

45. J. Nunnari and A. Suomalainen, "Mitochondria: In Sickness and in Health," *Cell* 148, no. 6 (2012): 1145–1159.

46. Y. Xin and Y. Zhang, "Paralog-Based Synthetic Lethality: Rationales and Applications," *Frontiers in Oncology* 13 (2023): 1168143.

47. "The Human Protein Atlas Webpage," accessed January 15, 2025, https://www.proteinatlas.org/.

48. M. Uhlén, L. Fagerberg, B. M. Hallström, et al., "Tissue-Based Map of the Human Proteome," *Science* 347, no. 6220 (2015): 1260419.

Supporting Information

Additional supporting information can be found online in the Supporting Information section. **Figure S1:** VRK1 gene expression was higher in SCNEC compared to that in AC patient-derived organoids. **Figure S2:** p53 status in the cell lines used. **Figure S3:** Representative images of subcutaneous tumors. **Figure S4:** VRK1 knockdown was maintained in mouse xenograft tumors throughout the observation period. **Figure S5:** Ki-67 and cleaved caspase-3 immunohistochemistry staining in TC-YIK xenografts. **Figure S6:** GSEA revealed that VRK1 was associated with mitochondrial function. **Figure S7:** Representative images of COX IV immunohistochemistry staining corresponding to H-scores of 0 (negative), 1 (weak), 2 (moderate), and 3 (strong). **Figure S8:** COX IV immunohistochemistry staining for mouse xenograft tumors derived from TC-YIK. **Figure S9:** GSEA revealed that VRK1 was associated with the regulation of responses to external stimuli. **Figure S10:** Nutrient deprivation did not alter the relationship between VRK1 and cell proliferation. **Figure S11:** Hypoxic conditions did not alter the relationship between VRK1 and cell proliferation. **Figure S12:** VRK1 knockdown in TC-YIK cells increased sensitivity to H_2O_2 in a dose-dependent manner. **Figure S13:** Western blot analysis detecting the expression levels of mitochondria-related proteins and the levels of epigenetic histone marks in TC-YIK cells treated with or without 50 μM H_2O_2 for 6 h. **Figure S14:** Subcellular localization of VRK1 in HCSC-1 cells as determined by immunocytochemistry. **Figure S15:** VRK2 expression was lower in SCNEC than that in SCC and AC. **Figure S16:** No normal tissue exhibited VRK1-VRK2 expression patterns similar to those of SCNEC. **Table S1:** Summary of the antibodies used in this study. **Table S2:** Three target-specific VRK1 constructs in shRNA lentiviral particles. **Table S3:** Conditions for colony formation assay. **Table S4:** Clinical characteristics of SCNEC, SCC, and AC cases. **Table S5:** HPV status of cell lines. **Table S6:** Gene set enrichment analysis results for shCont vs. shVRK1 RNA-seq data from HCSC-1 cell line-derived mouse subcutaneous tumors. **Table S7:** Gene set enrichment analysis results for shCont vs. shVRK1 RNA-seq data from TC-YIK cell line-derived mouse subcutaneous tumors. **Data S1:** Supplementary material and methods.